Chemical Gradients on Graphene To Drive Droplet Motion

Sandra C. Hernández,[#,*,⊥] Charlee J. C. Bennett,[†] Chad E. Junkermeier,[#,§] Stanislav D. Tsoi,[‡] Francisco J. Bezares,[▽,§] Rory Stine,[†] Jeremy T. Robinson,[§] Evgeniya H. Lock,[⊥] David R. Boris,[⊥] Brian D. Pate,[∥] Joshua D. Caldwell,[§] Thomas L. Reinecke,[§] Paul E. Sheehan,[‡,*] and Scott G. Walton[⊥,*]

[†]Nova Research Inc., 1900 Elkins Street, Suite 230, Alexandria, Virginia 22308, United States , [‡]Chemistry Division, Naval Research Laboratory, Washington, D.C. 20375, United States , [§]Electronics Science and Technology Division, Naval Research Laboratory, Washington, D.C. 20375, United States , [⊥]Plasma Physics Division, Naval Research Laboratory, Washington, D.C. 20375, United States, [∥]Joint Science and Technology Office for Chemical and Biological Defense, Defense Threat Reduction Agency, Fort Belvoir, Virginia 22060, United States , [#]NRC Postdoctoral Research Associateship Program, Naval Research Laboratory, Washington, D.C. 20375, United States, and [▽]ASEE Postdoctoral Research Associateship Program, Naval Research Laboratory, Washington, D.C. 20375, United States

ABSTRACT This work demonstrates the production of a well-controlled, chemical gradient on the surface of graphene. By inducing a gradient of oxygen functional groups, drops of water and dimethyl-methylphosphonate (a nerve agent simulant) are "pulled" in the direction of increasing oxygen content, while fluorine gradients "push" the droplet motion in the direction of decreasing fluorine content. The direction of motion is broadly attributed to increasing/decreasing hydrophilicity, which is correlated to high/low adhesion and binding energy. Such tunability in surface chemistry provides additional capabilities in device design for applications ranging from microfluidics to chemical sensing.

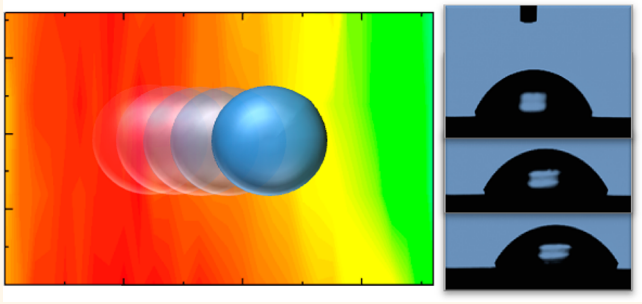

KEYWORDS: graphene · chemical gradient · droplet motion · plasma functionalization · chemical force microscopy · surface energy · adhesion,

The exceptional mechanical, optical, and electronic properties of graphene have motivated a vast amount of research.[1,2] While many scientific and technological opportunities remain for pristine graphene, interest has grown in the controlled functionalization of the surface chemistry to enhance its capabilities.[3] Fortunately, the flexibility of carbon chemistry provides many avenues for tuning the surface chemistry and nascent attempts have already significantly modulated the electronic, mechanical and chemical properties of graphene, pointing to an even broader potential range of applications in electronics,[4−7] mechanical resonators,[8] and bio/chemical sensing.[9−12] Critical to many applications is the ability to manipulate the reactivity, wettability and adhesive properties of graphene,[13−15] all of which are achievable by the introduction of functional groups.

While the global chemical modification of surfaces has many uses, controlling the spatial distribution of functional groups provides even greater functionality in that these functional groups can serve to convey the flow of adsorbates. Such surface engineering may lead to pump-free microfluidics, two-dimensional chemical preconcentrators, and site-specific receptor points in sensing applications. For example, Chaudhury *et al.* demonstrated that chemical gradients formed using silane chemistry on silicon dioxide could induce a water droplet to "run uphill".[13] Given the flexibility of carbon chemistry, graphene provides many options in designing such gradients. Moreover, to effectively move a liquid droplet, the surface chemistry gradient must be both continuous (*x* and *y* direction) and uniform in the direction perpendicular to the droplet motion (*y* direction) to prevent discontinuous areas that can pin the moving droplet. Manipulating the surface chemistry of graphene requires a delicate touch and thus the method to produce such a gradient must be carefully considered.

There are many successful approaches toward the chemical modification of graphene

* Address correspondence to sandra.hangarter.ctr@nrl.navy.mil, scott.walton@nrl.navy.mil, paul.sheehan@nrl.navy.mil.

Received for review September 15, 2012 and accepted May 9, 2013.

Published online May 09, 2013
10.1021/nn304267b

including *in situ* elemental doping,[16,17] wet[17−24] and dry[25] chemical treatment, thermal lithography[26] and plasma processing.[27−29] Of these, plasmas are an attractive method since they form the basis of processing schemes capable of imparting submicrometer-scale features over large areas.[30] In particular, electron-beam generated plasmas can introduce different functional groups over a range of coverage without etching of the carbon backbone.[27,31,32] The key to such control is the inherently low energy ions delivered to the surface.[33] As such, they provide a robust, yet agile tool for producing large-area graphene films with uniform and controlled surface chemistry.

The immediate interest of this work was to achieve a sufficiently high-quality gradient, of fluorine- or oxygen-rich chemical functional groups on graphene and to utilize the graded surface chemistry for directing the transport of liquid droplets. This work demonstrates that with careful consideration of the surface chemistry, electron beam-generated plasmas can be used to form a smooth oxygenated or fluorinated chemical gradient that can either "push" or "pull" droplets of water or dimethyl-methylphosphonate (DMMP, a nerve agent simulant), across the graphene surface.

RESULTS AND DISCUSSION

Grading of the chemical functional group density was achieved by use of a physical mask with a small gap structure (canopy shape) during plasma processing (Figure 1A). One of the unique features of plasmas is their ability to "mold" around structures, with this molding being proportional to the plasma density. As the plasma molds around the canopy, ions and electrons are lost to the surrounding walls. This causes a decrease in plasma density, which results in a gradual penetration under the canopy, and therefore provides control over both the total and relative number of ions and reactive neutrals incident on the underlying substrate.[34] Thus, adjusting the height of the canopy relative to the graphene surface, the canopy length, and/or the thickness of the canopy, the concentration and spatial distribution of the functional groups on the surface of graphene can be controlled. Figure 1 presents the spatial variation in total oxygen and fluorine content obtained using a mask with a 1 mm thick canopy, positioned 1 mm above the graphene surface that extends 15 mm from the base laterally. In each case, there is a region of the graphene surface, spanning roughly the first 5 mm from the base where the plasma density is highly depleted resulting in minimal modification (region I). Followed by a region of varying surface modification that spans roughly $5 \leq x \leq 15$ mm from the base (region II), and a fully exposed region extending from the end of the canopy ($x > 15$ mm from the base) resulting in heavy modification (region III).

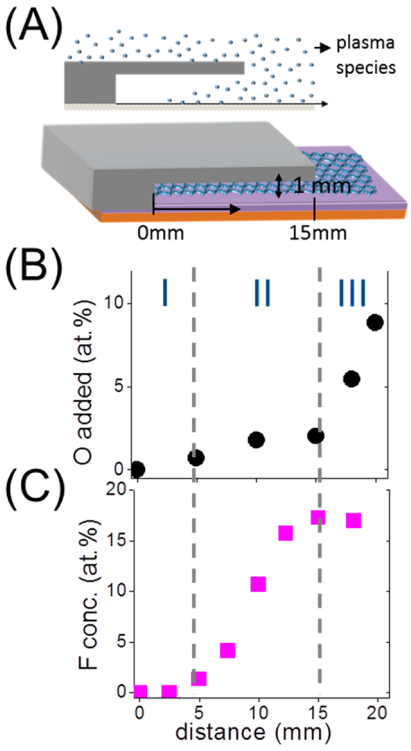

Figure 1. (A) Schematic representation of the canopy mask and the plasma processing architecture used and schematic of the plasma density profile, along with the (B) oxygen and (C) fluorine gradients produced with the canopy mask. Region I indicates areas that were fully covered by the canopy, region II indicates partially covered areas, and region III indicates areas that were fully exposed to the plasma.

The concentration of the added functional groups varied from 0 to 10 atomic % of oxygen (Figure 1B) and 0 to 17 atomic % of fluorine (Figure 1C) as determined by XPS. In particular, a rapid increase in concentration occurs in region III for oxygen and in region II for fluorine, which we attribute to differences in the plasma chemistries and plasma surface interactions.

The progression of functionalization along the chemical gradients on graphene is demonstrated in Figure 2 using conventional Raman spectroscopy (Figure 2A,C) to track the change from sp^2 to sp^3 hybridization[35] and XPS (Figure 2B,D) to determine the concentration of the added functional groups at the same locations. As shown in Figure 2A,C, the increased sp^3 hybridization that is induced with the greater functional group density leads to an intensification of the graphene "D" (1350 cm^{-1}) peak while reducing the "G" (1570 cm^{-1}) and "2D" (2700) peak intensities going from the unexposed to the completely exposed regions (regions I to III). As expected, the most striking changes of the D, G, and 2D peaks occur at the outer edge of the canopy where the fully exposed areas (region III) begin, a result that agrees with the abrupt increases in oxygen and fluorine surface concentration in Figure 1.

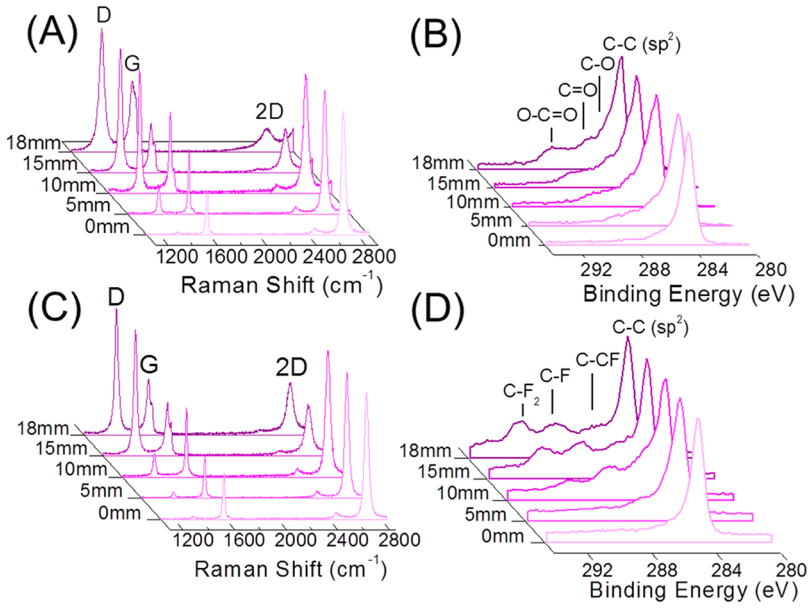

Figure 2. (A) Single point Raman measured along the oxygen gradient on graphene, and (B) the corresponding high-resolution C1s spectra. (C) Single point Raman and (D) high-resolution C1s of a fluorine gradient. All spectra are normalized to the maximum intensity.

Figure 2B,D shows the C1s XPS spectra for oxygen and fluorine gradients. In the case of an oxygen gradient (Figure 2B), the covered region preserves the sp^2 C−C (284.4 eV) bonding with a slight asymmetry associated to the presence of oxygen, likely incorporated during the transfer from the copper foil to the substrate (verified by XPS spectra taken before plasma processing). Moving toward region II, the C−C peak broadens due to the incorporation of C−O (285.8 eV) and then C═O (287.3 eV) functionalities.[36] In region III (at the edge of the canopy), the concentrations of the C═O and O−C═O species increased further, suggesting single bonded oxygen under the canopy and an increasing amount of carbonyl groups in the regions with higher plasma exposure. Similarly, the fluorine concentration (Figure 2D) increases moving from the canopy base to more exposed regions. The well-covered region I shows primarily sp^2 C−C, while the exposed regions (II and III) have C−CF (286.1 eV), C−F (288.6 eV), C−F_2 (290.8 eV) and C−F_3 (292.82 eV) functional groups with increasing concentrations as the plasma density at the graphene surface was increased.

The chemical gradient continuity and lateral uniformity may be ascertained using micro-Raman and XPS mapping over areas of about 2 mm × 20 mm. Note that measurement positions are approximate since the measurements were taken in two separate instruments with substantially different sampling areas (4 μm for Raman *vs* 400 μm for XPS) and without the benefit of fiduciary marks. In the case of Raman spectroscopy, the comparison of the graphene D to G ratio provides a measurement of the electron correlation length, which in turn provides a good figure of merit for the quality of the graphene film.[35] Presented in Figure 3A−C are μ-Raman maps showing the D/G peak intensity ratios of pristine and chemically modified surfaces along the gradients. Generally, before plasma exposure (Figure 3A), the graphene surface exhibits a low D/G ratio, indicative of high quality graphene, as evidenced by the uniform distribution of the D/G ratio in the range of about 0.03. After plasma exposure, the oxygen gradient map in Figure 3B shows a gradual increase in the D/G ratio from 0.03 to about 3 going from covered to exposed regions with only slight variations in the direction perpendicular to the chemical gradient, indicating that the structural modification was well controlled over large areas. On the other hand, the fluorinated gradient surface (Figure 3C) demonstrates minimal structural changes from region I to II, followed by a pronounced increase in the D/G ratio from 0.01 to about 2 going from region II to III. This is in contrast to the XPS data that shows the presence of fluorine containing functionalities after 5 mm. There are several factors that can contribute to the different structural and chemical modifications for either an oxygen-rich or fluorine-rich gradient. The gradients produced *via* plasma exposure are influenced by the plasma chemistries and plasma-surface interactions that each plasma provides.[37] While the experimental configuration and operating conditions are similar, the type, amount, and spatial profile of species added to the graphene surface and the associated structural changes are different. These differences can be attributed to differences in bonding types and their influence over the resulting structural configuration of graphene. Oxygen functionalities, for example, will pull the attaching carbon

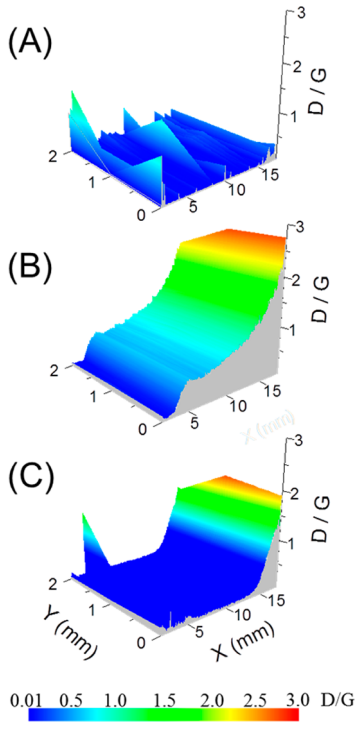

Figure 3. Micro-Raman maps showing the D/G ratio of (A) a graphene surface before functionalization, (B) an oxygen gradient, and (C) a fluorine gradient graphene surface. The step and spot size were 50 μm and ~2 μm, respectively. The D/G intensity increases from blue to red, with the actual intensity given on the *z*-axis of each map; a contour bar is provided at the bottom of the figure.

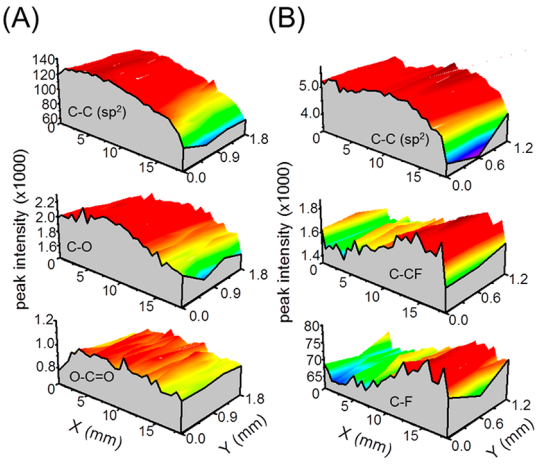

Figure 4. XPS chemical maps of select components of the high resolution C1s for (A) an oxygenated gradient surface, and (B) a fluorinated gradient surface. The step and spot size were 600 and 400 μm, respectively. Generally, intensity increases from blue to red, with the actual intensity given on the *z*-axis of each map.

atom from the graphene plane more aggressively, leading to significant structural changes at the functionalized sites.[38] Fluorine functionalities however, can maintain sp^2 hybridization at low F coverage,[39] while sp^3 configuration is expected at larger F coverage because the F−C bond can acquire an ionic character making it more covalent-like.[40] Raman spectroscopy is very sensitive to structural changes; therefore, at comparable surface coverage, oxygen functionalities show more pronounced D peaks (higher D/G ratios) since they perturb the sp^2 hybridization more drastically than fluorine functionalities.

The distribution of functional group type over the same sample area was mapped using XPS chemical imaging of the C1s region (Figure 4). For both functionalizations, the concentration of C−C sp^2 decreases monotonically along the gradient away from the protected area. As expected, the sp^2 decrease is accompanied by an increase in functional group concentration; although, not all groups increase uniformly. For example, both C−O and C═O are most prevalent in the midportion of the gradient (regions I to II), whereas O−C═O functionalities are most prevalent at the canopy edge (region II to III). For the fluorine gradient (Figure 4B), the presence of C−CF, C−F, and C−F_2 functionalities all appear near the end of the canopy (region II to III and the full extent of region III). Here again, the maps confirm a reasonably uniform distribution of functional groups suggesting uniform chemical distribution in the direction perpendicular to the gradient (*y* direction). Combined with spot XPS measurements (Figure 1 and 2), these maps suggest the gradients vary not only in total oxygen and fluorine content, but also in moiety type, with concentration and complexity increasing toward the fully exposed regions.

A gradient in the surface chemistry is necessary to produce an effective shift in the surface's interaction with the liquid. As a first step in understanding these interactions, contact angle measurements of untreated graphene and uniformly functionalized graphene (blanket coverage) were performed. Contact angle measurements average the influence of the substrate[41] as well as inherent defects such as wrinkles and grain boundaries present on graphene but still provide reasonable global information on the hydrophobicity, a measure of the system's overall surface energy. By acquiring contact angles using a series of polar and nonpolar liquids, the Lewis acid−base and nonpolar components of the free energy can be obtained. The influence of functional groups on the contact angle of water and DMMP is shown in Figure 5. Note that the various graphene surfaces were placed on the same type of substrate (SiO_2/Si with oxide thickness of 100 nm). Graphene transferred onto SiO_2 had a H_2O contact angle of 94.8°, which is consistent with previous measurements[36] and with a surface energy of ≈38 mJ/m^2 (Figure 5A). Both values changed dramatically after the addition of functional groups, with the change in surface energy driven almost entirely by the adhesive components of the surface energy.[42] Functionalizing with oxygen (≈11 atom %) made the surface more hydrophilic, *reducing* the contact angle to 29.1°, and increasing the surface energy to 46.8 mJ/m^2. In contrast, the addition of fluorine slightly

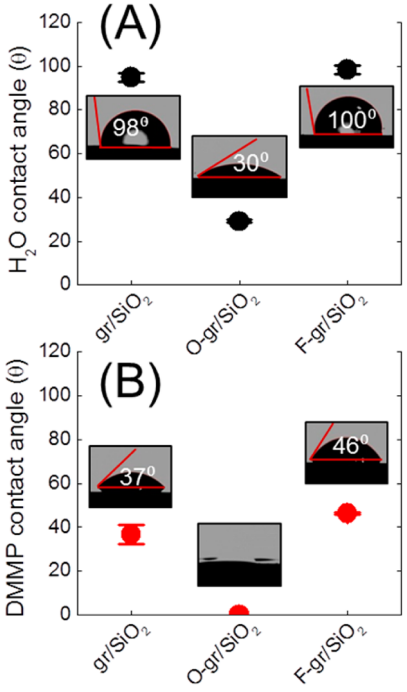

Figure 5. Contact angles of 1 μL drops of (A) water and (B) DMMP on pristine and chemically modified graphene surfaces.

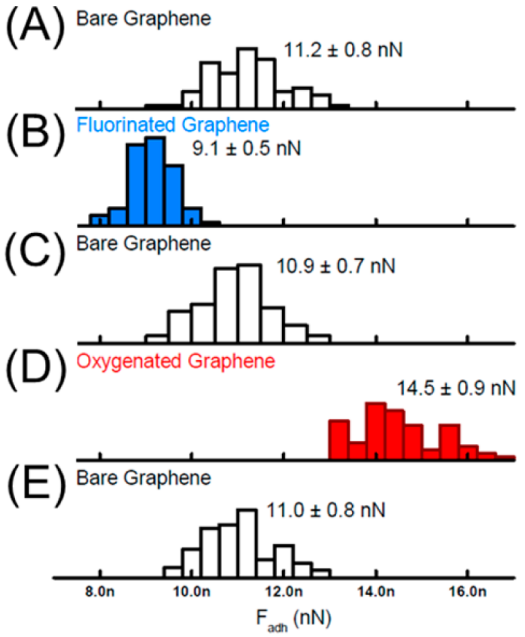

Figure 6. Distributions of adhesion forces measured between a DEPA-functionalized silicon nitride cantilever and unfunctionalized/functionalized graphene surfaces supported by SiO_2. The principal values were determined by Gaussian fits and the uncertainties given by standard deviation.

increased the hydrophobicity with a corresponding increase in the contact angle (≈100°) and decrease in surface energy (31.8 mJ/m^2). The wettability of graphene by DMMP is similar to the observed behavior with water, wherein the addition of oxygen functionalities enhanced the hydrophilicity of the graphene by DMMP to nearly complete wetting (Figure 5B) and the presence of fluorine made the surface less wetting. This is not surprising due to the polar nature of DMMP, which will induce similar hydrogen bonding interactions as observed with water. Changes in surface free energy of graphene are achieved by varying the type and coverage of functional groups, thereby controlling the strength of its interaction with other liquids, clearly demonstrating the tunability of the graphene surface chemistry.

While contact angle measurements provide a view of the global interactions, a more detailed view may be obtained through chemical force microscopy (CFM). In CFM, an AFM cantilever is functionalized with a specific chemical group, and the modified cantilever is then brought in contact with a desired surface. This method is used to elucidate surface interactions (adhesion) of the specific chemical group and a target surface. Here, an AFM cantilever was coated with diethylphosphonoacetic acid (DEPA) through its carboxyl group leaving the P atom and O bonds accessible to the graphene surface. DEPA is structurally similar to DMMP and can be covalently bound to the cantilever tip, while exposing its P atom and three O bonds (polar portion of the molecule) toward the graphene surface. The force of adhesion (F_{ad}) was determined by the force required to separate the modified tip from the contacted surface. Adhesion forces measured with the modified tip on pristine and functionalized graphene surfaces are presented in Figure 6. To ensure consistency of the measurements, adhesion forces were recorded on the pristine graphene surface before and after measurements on each functionalized surface (Figure 6A,C,E). The reproducibility of the adhesion force on the pristine surface indicates that the tip was not modified between the measurements. Relative to pristine graphene, the DEPA coated tip adheres less to the fluorinated graphene (Figure 6B) and adheres more to the oxygenated graphene surface (Figure 6D), which is consistent with the increased surface energy of the oxygenated graphene and the decreased surface free energy of the fluorinated surface in comparison to the pristine graphene.

Adhesive forces can have contributions from van der Waals interactions and from acid−base (usually hydrogen-bonding) interactions. Neither the pristine nor the fluorinated graphene surfaces should participate in strong acid−base interactions; therefore, adhesion to these surfaces may be attributed to the van der Waals interactions only. Because graphene represents a very thin layer on the SiO_2 substrate and the DEPA forms a similarly thin layer on the silicon nitride tip, the long-distance van der Waals forces are predominantly due to interactions between the SiO_2 surface and silicon nitride tip. It is common to approximate the AFM tip as a sphere of radius R in analytical models which allows the attractive van der Waals force between it and the

substrate to be simply written as $F_{vdW} = -(A_H R/6D^2)$, where A_H is the Hamaker constant and D is the tip−substrate separation. As the van der Waals interactions on the pristine and fluorinated graphene are dominated by the SiO_2 substrate, both should have identical Hamaker constants. Consequently, the weaker adhesion of the contacted tip to the fluorinated graphene must be due to an increase in separation D, possibly due to steric effects of the fluorine functional groups that extend above the graphene surface and thus push adsorbed DEPA molecules away compared to pristine graphene. Oxygenated graphene and the DEPA-functionalized tip form extensive hydrogen bonds in addition to the aforementioned van der Waals interactions. This is reflected in the increased adhesion of the tip to the oxygenated graphene. These results show that the adhesion force varies depending on the functional group where $F_{fluorinated} < F_{bare} < F_{oxygenated}$.

Modelistic approaches in combination with density functional theory (DFT) calculations were used to gain some insight into the qualitative trends of microscopic interactions with these surfaces. There are many possibilities for O and F functionalized graphene structures, as well as positions and orientations for the DMMP adsorbate. For simplicity, the orientation of the DMMP molecule in the calculations was kept to that suggested by the CFM measurements (see Materials and Methods for details). Generally, the adsorption energies calculated for DMMP on the fluorinated surfaces were found to be smaller than those for pristine graphene, and for oxygenated graphene were found to be greater than those for pristine graphene. Examples are shown in Figure 7. This is consistent with the CFM measurements which measured smaller adhesion on fluorinated graphene than on oxygenated graphene. The ordering of adsorption energies is also similar to those seen in the contact angle measurements in which the fluorinated surface was found to be less chemically active and the oxygenated surface more chemically active than for pristine graphene. In combination, this suggests that the observed adsorption and chemical activity of the surfaces could arise from microscopic interactions similar to those in the models of F and O functionalization used in the DFT calculations.[43−47] Since the contact angle, CFM measurements and DFT calculations encompass different scales, the DFT calculations presented here are intended to provide only a qualitative interpretation of the experimental data.

Chemical gradients that are sufficiently smooth and steep can move liquids.[25,26] Chemical velocity profiles of water and DMMP on fluorinated and oxygenated surfaces are presented in Figures 8 and 9, respectively. These results indicate that graphene may be modified to either "pull" or "push" droplets of water or DMMP. For these measurements, the graded graphene sample

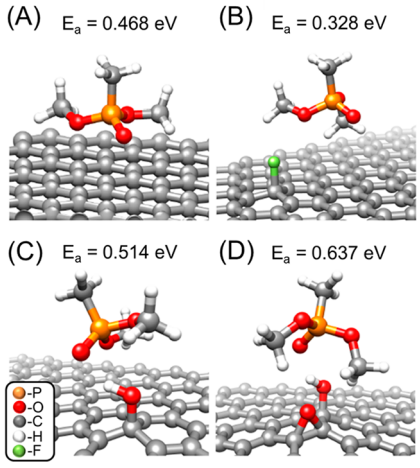

Figure 7. Examples of DMMP adsorbed on (A) pristine graphene. Configurations (B) at a fluorine adsorbate on graphene, (C) at a hydroxyl adsorbate on graphene, (D) at a pair of hydroxyl and epoxy adsorbate on the surface of graphene.

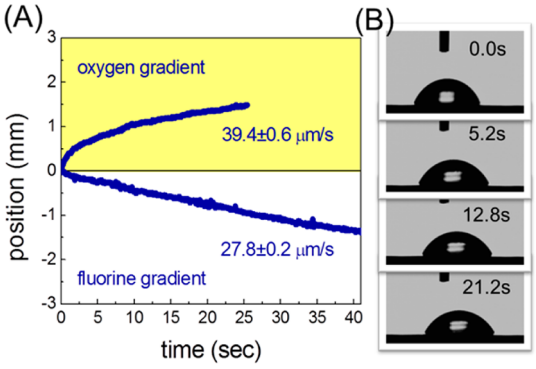

Figure 8. (A) Velocity profiles of H_2O droplets on oxygen (yellow) and fluorine gradient surfaces, and (B) still pictures of the droplet motion for H_2O on an oxygen gradient.

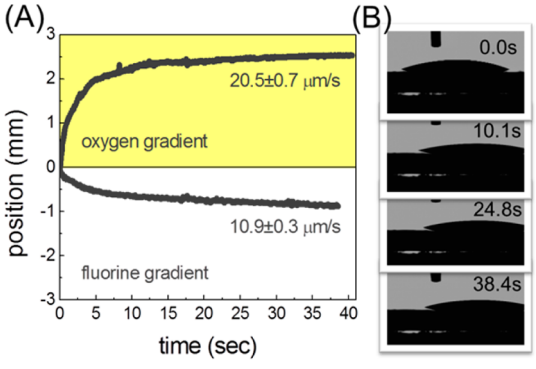

Figure 9. (A) Velocity profiles of DMMPdropletson oxygen (yellow) and fluorine gradient surfaces, and (B) still pictures of the droplet motion for DMMP on an oxygen gradient.

was placed on a level stage and a water droplet was placed on the area where the oxygen or fluorine concentration changes abruptly (see Figure 1, region III).

The motion of the droplet was monitored from the side as it moved along the gradient. Monitoring the droplet motion from above to measure displacement both parallel and perpendicular to the gradient would increase the accuracy of the measurement but was not possible with the current apparatus. However, we do note that the droplet did not move out of focus during its traverse, so its displacement perpendicular to the gradient was always significantly less than along the gradient. Figure 8B shows the water droplet as it moves spontaneously on an oxygen gradient toward the direction of the higher oxygen content. Similarly, when a droplet of DMMP was placed on the same oxygen gradient surface, it moved toward the more oxygen rich region (Figure 9B). To ensure that the movement was propelled by the oxygen gradient, the sample was rotated 180° and the experiment was repeated. Again, the droplets moved toward the highest oxygen content region. In the case of a fluorinated gradient, both droplets moved away from the fluorine rich region.

The droplets moved a total of 1−3 mm in one direction being "pulled" by the oxygen gradient or "pushed" by the fluorine gradient, with respect to the highest oxygen or fluorine content. The velocity slope trends in Figure 8A and Figure 9A reflect the "pulling" of the droplets on oxygenated graphene, where the droplet moved in the direction of increasing oxygen concentration signaling a positive trend in the slope. Similarly the "pushing" of the droplets on fluorinated graphene occurs in the direction of decreasing fluorine concentration signaling a negative trend in the slope. Typically, droplet motion occurred in two regimes;[48,49] with an initial fast relaxation of the drop shown in the nonlinear portion of the velocity profile. The droplet then enters a second regime of constant velocity, where the droplet creeps for the remaining time recorded. For the oxygen gradient, the water velocity was 39.4 ± 0.6 μm/s and the DMMP velocity was 20.5 ± 0.7 μm/s. For the fluorine gradient, the velocities were less, with values of 27.8 ± 0.2 μm/s for water and 10.9 ± 0.3 μm/s for DMMP. The volume changes in the droplets were monitored during motion and were determined to be minimal.

The direction of motion and droplet velocity can be broadly described in terms of increasing/decreasing hydrophilicity and the interaction with the varying functional group moieties, which is correlated to high/low adhesion and binding energy. The presence of oxygen produces a more hydrophilic surface, with higher surface energy, and increased adhesion; and thus, motion toward the region of higher oxygen concentration. The opposite is true in the presence of fluorine, where fluorine creates a more hydrophobic surface and thus a lower surface energy that is correlated to a decrease in adhesion and a decrease in adsorption energy, which explains the observed fluid motion away from the highly fluorinated region. Given that water has a dipole moment of 1.85 D and DMMP of 2.86−3.62 D,[50−53] the hydroxyl groups of the oxygenated graphene gradient most likely interacts with the positive polar components of water (-H groups) and DMMP (P−O group) through hydrogen bonding. However, since the available oxygen is bonded to the graphene structure in the form of C−O, C═O and O−C═O functionalities, the interaction between the liquid drops and the oxygen functionalities is most likely through hydrogen interactions. The lower velocities on the fluorine gradient are consistent with the greater change in surface energy and adhesion forces with oxygen functionalization than with fluorine functionalization (Figure 5). That is, the gradient in surface energy is greater in the oxygen gradient than in the fluorine gradient and so should provide an overall greater driving force. In either case, the chemistry provided the means for fluid transport across the chemically graded graphene surface, therefore, demonstrating the concept of chemically modified graphene as a substrate to induce chemical movement.

CONCLUSIONS

This work demonstrates the ability to produce chemical gradients on graphene using a physical mask during plasma processing and the use of those gradients to induce motion of chemical species. The plasma process yields chemical gradients that vary not only in total oxygen or fluorine content but also in moiety type, with good lateral functional group uniformity. Oxygen gradients were shown to "pull" drops of water and DMMP in the direction of increasing oxygen content, while fluorine gradients were shown to "push" such droplets in the direction of decreasing fluorine content. The direction of motion and droplet velocity can be broadly described in terms of increasing/decreasing hydrophilicity, which is correlated to high/low adhesion and binding energy in chemical force microscopy measurements and in density functional calculations. The plasma-based process of gradient production is flexible enough to accommodate a range of surface chemistries and coverages that could be used to further tailor performance.

To place the results in a larger context, we note that the flexible fabrication of chemical gradients in graphene is made more significant in that graphene can be transferred to arbitrary substrates. To date, methods for fabricating gradients (and changing surface functionality in general) have broadly relied on covalent attachment between a SAM forming molecule such as alkanethiols or silanes and the substrate. With graphene, there is the potential to form gradient or chemical

patterns on a film which may then be transferred to other substrates, effectively decoupling a working sensor or detector substrate from the necessary chemistry. Decoupling the chemistry from the device material should enable much greater freedom in device design for applications ranging from microfluidics to sensing.

MATERIALS AND METHODS

Graphene Growth and Transfer. Graphene was produced by low-pressure chemical vapor deposition growth on copper foils,[54,55] then transferred to SiO_2/Si substrates using conventional techniques.[56] Briefly, copper-foil enclosures were heated to 1030 °C under flowing H_2 ($P_{H2}\approx$ 5 mTorr) and then methane was introduced ($P_{CH4}\approx$ 30 mTorr) for approximately 1 h ($P_{total}\approx$ 35−40 mTorr). After growth, samples were coated with a thin PMMA layer, and then, the Cu foil was removed by chemical etching in an ammonium persulfate solution. The PMMA/graphene film was then rinsed in a water bath and transferred to a SiO_2/Si substrate, followed by removal of the PMMA with acetone. Finally, the graphene/SiO_2/Si samples were thermally annealed up to 300 °C for 2 h in H_2/Ar ambient. Large area samples of continuous graphene films were confirmed by optical imaging. Cleanliness and integrity of the graphene was verified using XPS and Raman spectroscopy. In particular, only samples exhibiting a nearly symmetric C−C (sp^2) spectra and without a significant D peak were used as starting materials.

Plasma Processing. Pulsed electron-beam generated plasmas were produced by injecting a 2 keV electron beam into a background gas. The electron beam is produced by applying a −2 kV pulse to a linear hollow cathode. The beam emerges from the hollow cathode and passes through a slotted anode, and terminates at a second grounded anode located further downstream. The resulting electron beam is magnetically confined, to minimize spreading, producing a sheet-like plasma in background gases of O_2/Ar, or SF_6/Ar mixtures to produce the desired functionalities.[32] The system base pressure is maintained at $\sim 1 \times 10^{-6}$ Torr prior to processing by a turbo molecular pump. Reactive gases are introduced at 5% of the total flow rate (180 sccm) with argon providing the balance to achieve an operating pressure of 90 mTorr. For this work, the pulse width was 2 ms and the duty factor was maintained at 10%. Graphene samples were placed on a processing stage adjacent to the plasma at a distance of 2.5 cm from the electron-beam axis. All processing was performed at room temperature. To produce chemical gradients, aluminum, canopy masks with geometries described in Figure 1 were used. The masks were mounted on the processing stage such that the graphene samples sat underneath the overhang, thus ensuring a variable plasma exposure with partially to completely exposed regions. Blanket coverage of the graphene samples were produced without the mask.

Surface Characterization. XPS analysis was performed using a monochromatic X-ray photoelectron spectrometer (K-Alpha XPS System). Surface composition was determined by fitting the high resolution elemental spectra of the C1s, F1s and O1s peaks using commercially available Unifit software. Subcomponents of the C1s region were identified by first fitting the lowest binding energy component (sp^2 C−C) and restricting the full-width-half-maximum of that component to all other components. Subcomponents were assigned by their binding energy and relative distance to the lowest binding energy component. XPS chemical maps of functionalized graphene surfaces were obtained over an area of ~2 mm × 20 mm, at a step size of 600 μm and a spot size of 400 μm. Traditional Raman characterization was performed using an InVia Raman microscope (Renishaw) equipped with a 50× objective lens, a 514.5 nm diode laser excitation, at a set power of 20 mW at the source with a spot size of 5 μm. The Raman scattered light was dispersed using a scanning 1800 groove/mm grating on a photomultiplier tube.

Raman mapping was carried out using a custom system operating with a 514 nm laser light provided by a Coherent Innova 90−5 Argon-Ion laser that was focused on the sample through a 100×, 0.75 NA objective attached to a Mitutoyo microscope. Analysis was performed at a set laser power of approximately 40 mW with a spot-size of approximately 2 μm, and a signal acquisition time of 10 s. Spatial mapping of the Raman intensities of the graphene peaks was performed using a Prior Scientific ProScan II automated stage mounted to the microscope using a step size of 50 μm. Power dependence measurements were performed prior to measuring the samples to ensure damage free data acquisition during the μ-Raman mapping.

Contact Angle Goniometry and Surface Energy Estimation. Static and dynamic contact angle measurements were performed using an automated digital goniometer (AST Producs, Inc.) equipped with a dispersing needle holder. Liquids with known surface properties (water, ethylene glycol, and diiodomethane) were placed on the graphene with a microsyringe dedicated for each liquid. Once the microsyringe is inserted in the needle holder, a 1 μL droplet is extruded while the graphene is raised perpendicular to the needle holder. Contact angles of both sides of three independent drops were averaged for each sample. The surface energy was estimated using the van Oss-Chaudhury-Good model.[57] Videos of 1 μL of water and 2 μL of dimethylmethylphosphonate (DMMP) were collected over 30−60 s on a level surface.

Force Adhesion. For chemical force microscopy measurements, silicon nitride AFM probes were functionalized by first exposing them to a glow discharge plasma containing humidified air. This process forms, among other species, a number of primary amines on the nitridesurface[58] that can then covalently bind organic molecules. Here, the probes were functionalized with diethylphosphonoacetic acid (DEPA), a molecule structurally similar to DMMP that contains a diethylphosphonate head group but also a carboxyl group for coupling to the primary amines. The aminated tips were submerged for 2 h in a 50 mM solution of DEPA containing excess ethyl(dimethylaminopropyl)carbodiimide (EDC) and *N*-hydroxysuccinimide (NHS) in 0.1 M MES buffer (pH 5.4), then rinsed with deionized water and ethanol. The EDC and NHS react with the carboxyl group of DEPA to form an *N*-hydroxysuccinimidyl ester, which can then covalently couple with the amine groups on the surface of the AFM tip. XPS spectra taken on a witness piece of silicon nitride showed the appearance of a P 2p peak as well as a carbonyl peak in the C 1s spectra, both indicative of the addition of DEPA to the surface.

Chemical force microscopy (in contact mode) was performed on an enclosed Cypher Atomic Force Microscope/Scanning Probe Microscope (Asylum Research, Inc.) under dry nitrogen with residual oxygen measured at 0.3%. Force adhesion curves were acquired by the silicon nitride probe (Asylum Research, Inc.) with a calibrated spring constant of 0.742 N/m. Measurements on all surfaces were taken at a scan rate of 0.5 Hz and a force distance of 1 μm. To allow for meaningful data comparisons, all three (pristine, oxygenated, fluorinated graphene) surfaces were probed with the same cantilever tips and the data normalized. Additionally, the pristine graphene surface was probed after each functionalized graphene surface to confirm consistency of the measurements. Stacked histograms of multiple scans were compiled from raw data and the average adhesion force on each surface was calculated *via* statistical analysis.

Calculations. Calculations of the electronic and structural properties of models of the functionalized surfaces were done to gain qualitative insight into the trends of the energetics and structures of DMMP binding on graphene with fluorine and oxygen. The calculations were made with the Quantum Espresso package,[59,60] a kinetic energy cut off of 30 Ry for the plane waves, the Perdew-Burke-Ernzerhof exchange-correlation, Vanderbilt ultrasoft,[61] semiempirical dispersion terms (DFT-D)[43−47] to treat the weak dispersive interactions (van der Waals interactions), and 8-by-8 supercell geometries. This approach was used in earlier studies of graphene with oxygen adsorption and graphene with fluorine adsorption.[25,61,62]

Models for the orientation of the DMMP molecules were used based on information from the CFM measurements. The DMMP was oriented above the graphene surface with the P atom above a graphene carbon atom, the oxygen in the (O═P) bond pointing toward a neighboring graphene C atom, and the C in the DMMP P−CH_3 bond pointing nearly vertically above the P atom (see Supporting Information).

Conflict of Interest: The authors declare no competing financial interest.

Acknowledgment. This work was supported by the Naval Research Laboratory Base Program and the Defense Threat Reduction Agency under MIPR number B112609M. S.C.H. and C.E.J. appreciates the support of the National Research Council. F.J.B. appreciates the support of the American Society of Engineering Education. S.C.H. would like to thank A. K. Noll for designing the physical masks and Dr. R. F. Fernsler for useful discussions on plasma/surface interactions.

Supporting Information Available: Details of the density functional theory (DFT) calculations for the structures, binding events, and positions described here can be found in the Supporting Information. This material is available free of charge *via* the Internet at http://pubs.acs.org.

REFERENCES AND NOTES

1. Geim, A. K. Graphene: Status and Prospects. *Science* **2009**, *324*, 1530–1534.
2. Rao, C. N. R.; Sood, A. K.; Subrahmanyam, K. S.; Govindaraj, A. Graphene: The New Two-Dimensional Nanomaterial. *Angew. Chem., Int. Ed.* **2009**, *48*, 7752–7777.
3. Wang, Q. H.; Jin, Z.; Kim, K. K.; Hilmer, A. J.; Paulus, G. L. C.; Shih, C.-J.; Ham, M.-H.; Sanchez-Yamagishi, J. D.; Watanabe, K.; Taniguchi, T.; *et al.* Understanding and Controlling the Substrate Effect on Graphene Electron-Transfer Chemistry *via* Reactivity Imprint Lithography. *Nat. Chem.* **2012**, *4*, 724–732.
4. Cho, S. J.; Chen, Y. F.; Fuhrer, M. S. Gate-Tunable Graphene Spin Valve. *Appl. Phys. Lett.* **2007**, *91*, 1231051–1231053.
5. Lin, Y. M.; Dimitrakopoulos, C.; Jenkins, K. A.; Farmer, D. B.; Chiu, H. Y.; Grill, A.; Avouris, P. 100-GHz Transistors from Wafer-Scale Epitaxial Graphene. *Science* **2010**, *327*, 662–662.
6. Robinson, J. A.; Hollander, M.; LaBella, M.; Trumbull, K. A.; Cavalero, R.; Snyder, D. W. Epitaxial Graphene Transistors: Enhancing Performance *via* Hydrogen Intercalation. *Nano Lett.* **2011**, *11*, 3875–3880.
7. Tombros, N.; Jozsa, C.; Popinciuc, M.; Jonkman, H. T.; van Wees, B. J. Electronic Spin Transport and Spin Precession in Single Graphene Layers at Room Temperature. *Nature* **2007**, *448*, 571–574.
8. Robinson, J. T.; Zalalutdinov, M.; Baldwin, J. W.; Snow, E. S.; Wei, Z.; Sheehan, P.; Houston, B. H. Wafer-Scale Reduced Graphene Oxide Films for Nanomechanical Devices. *Nano Lett.* **2008**, *8*, 3441–3445.
9. Baraket, M.; Stine, R.; Lee, W. K.; Robinson, J. T.; Tamanaha, C. R.; Sheehan, P. E.; Walton, S. G. Aminated Graphene for DNA Attachment Produced *via* Plasma Functionalization. *Appl. Phys. Lett.* **2012**, *100*, 2331231–2331234.
10. Robinson, J. T.; Perkins, F. K.; Snow, E. S.; Wei, Z.; Sheehan, P. E. Reduced Graphene Oxide Molecular Sensors. *Nano Lett.* **2008**, *8*, 3137–3140.
11. Schedin, F.; Geim, A. K.; Morozov, S. V.; Hill, E. W.; Blake, P.; Katsnelson, M. I.; Novoselov, K. S. Detection of Individual Gas Molecules Adsorbed on Graphene. *Nat. Mater.* **2007**, *6*, 652–655.
12. Stine, R.; Robinson, J. T.; Sheehan, P. E.; Tamanaha, C. R. Real-Time DNA Detection Using Reduced Graphene Oxide Field Effect Transistors. *Adv. Mater.* **2010**, *22*, 5297–5300.
13. Wang, S. R.; Zhang, Y.; Abidi, N.; Cabrales, L. Wettability and Surface Free Energy of Graphene Films. *Langmuir* **2009**, *25*, 11078–11081.
14. Shin, Y. J.; Wang, Y. Y.; Huang, H.; Kalon, G.; Wee, A. T. S.; Shen, Z. X.; Bhatia, C. S.; Yang, H. Surface-Energy Engineering of Graphene. *Langmuir* **2010**, *26*, 3798–3802.
15. Zhang, X. Q.; Wan, S. H.; Pu, J. B.; Wang, L. P.; Liu, X. Q. Highly Hydrophobic and Adhesive Performance of Graphene Films. *J. Mater. Chem.* **2011**, *21*, 12251–12258.
16. Guan, L.; Cui, L.; Lin, K.; Wang, Y. Y.; Wang, X. T.; Jin, F. M.; He, F.; Chen, X. P.; Cui, S. Preparation of Few-Layer Nitrogen-Doped Graphene Nanosheets by DC Arc Discharge Under Nitrogen Atmosphere of High Temperature. *Appl. Phys. A: Mater. Sci. Process.* **2011**, *102*, 289–294.
17. Wu, X. M.; Cao, H. Q.; Li, B. J.; Yin, G. The Synthesis and Fluorescence Quenching Properties of Well Soluble Hybrid Graphene Material Covalently Functionalized with Indolizine. *Nanotechnology* **2011**, *22*, 0752021–0752028.
18. Wang, Y.; Guo, C. X.; Wang, X.; Guan, C.; Yang, H. B.; Wang, K. A.; Li, C. M. Hydrogen Storage in a Ni-B Nanoalloy-Doped Three-Dimensional Graphene Material. *Energy Environ. Sci.* **2011**, *4*, 195–200.
19. Wang, Y.; Yao, H. B.; Wang, X. H.; Yu, S. H. One-Pot Facile Decoration of CdSe Quantum Dots on Graphene Nanosheets: Novel Graphene-CdSe Nanocomposites with Tunable Fluorescent Properties. *J. Mat. Chem.* **2011**, *21*, 562–566.
20. Yuchen, X.; Jian-guo, L.; Yong, Z.; Wenming, L.; Jian, G.; Yun, X.; Ying, Y.; Zhigang, Z. Preparation and Characterization of Pt Supported on Graphene with Enhanced Electrocatalytic Activity in Fuel Cell. *J. Power Sources* **2011**, *196*, 1012–1018.
21. Guan, L.; Cui, L.; Lin, K.; Wang, Y. Y.; Wang, X. T.; Jin, F. M.; He, F.; Chen, X. P.; Cui, S. Preparation of Few-layer Nitrogen-Doped Graphene Nanosheets by DC Arc Discharge Under Nitrogen Atmosphere of high temperature. *Appl. Phys. A: Mater. Sci. Process.* **2011**, *102*, 289–294.
22. Liu, X. W.; Mao, J. J.; Liu, P. D.; Wei, X. W. Fabrication of Metal-Graphene Hybrid Materials by Electroless Deposition. *Carbon* **2011**, *49*, 477–483.
23. Zhang, K.; Yue, Q. L.; Chen, G. F.; Zhai, Y. L.; Wang, L.; Wang, H. S.; Zhao, J. S.; Liu, J. F.; Jia, J. B.; Li, H. B. Effects of Acid Treatment of Pt-Ni Alloy Nanoparticles@Graphene on the Kinetics of the Oxygen Reduction Reaction in Acidic and Alkaline Solutions. *J. Phys. Chem. C* **2011**, *115*, 379–389.
24. Zhao, H.; Yang, J.; Wang, L.; Tian, C. G.; Jiang, B. J.; Fu, H. G. Fabrication of a Palladium Nanoparticle/Graphene Nanosheet Hybrid *via* Sacrifice of a Copper Template and its Application in Catalytic Oxidation of Formic Acid. *Chem. Commun.* **2011**, *47*, 2014–2016.
25. Robinson, J. T.; Burgess, J. S.; Junkermeier, C. E.; Badescu, S. C.; Reinecke, T. L.; Perkins, F. K.; Zalalutdniov, M. K.; Baldwin, J. W.; Culbertson, J. C.; Sheehan, P. E.; *et al.* Properties of Fluorinated Graphene Films. *Nano Lett.* **2010**, *10*, 3001–3005.
26. Wei, Z.; Wang, D.; Kim, S.; Kim, S.-Y.; Hu, Y.; Yakes, M. K.; Laracuente, A. R.; Dai, Z.; Marder, S. R.; Berger, C.; *et al.* Nanoscale Tunable Reduction of Graphene Oxide for Graphene Electronics. *Science* **2010**, *328*, 1373–1376.
27. Baraket, M.; Walton, S. G.; Lock, E. H.; Robinson, J. T.; Perkins, F. K. The Functionalization of Graphene Using Electron-Beam Generated Plasmas. *Appl. Phys. Lett.* **2010**, *96*, 2315011–2315013.
28. Baraket, M.; Walton, S. G.; Wei, Z.; Lock, E. H.; Robinson, J. T.; Sheehan, P. Reduction of Graphene Oxide by Electron Beam Generated Plasmas Produced in Methane/Argon Mixtures. *Carbon* **2011**, *48*, 3382–3390.
29. Kato, T.; Jiao, L.; Wang, X.; Wang, H.; Li, X.; Zhang, L.; Hatakeyama, R.; Dai, H. Room-Temperature Edge Functionalization and Doping of Graphene by Mild Plasma. *Small* **2011**, *7*, 574–577.
30. Engelmann, S. U.; Martin, R.; Bruce, R. L.; Miyazoe, H.; Fuller, N. C. M.; Graham, W. S.; Sikorski, E. M.; Glodde, M.; Brink, M.; Tsai, H.; *et al.* Patterning of CMOS Device Structures for 40−80 nm Pitches and Beyond. *Proc. SPIE* **2012**, *8328*, 83280B1–83280B12.
31. Hopkins, P. E.; Baraket, M.; Barnat, E. V.; Beechem, T. E.; Kearney, S. P.; Duda, J. C.; Robinson, J. T.; Walton, S. G. Manipulating Thermal Conductance at Metal-Graphene Contacts *via* Chemical Functionalization. *Nano Lett.* **2012**, *12*, 590–595.

32. Walton, S. G.; Hernández, S. C.; Baraket, M.; Wheeler, V. D.; Nyakiti, L. O.; Myers-Ward, R. L.; Eddy, C. R., Jr.; Gaskill, D. K. Plasma-Based Chemical Modification of Epitaxial Graphene. *Mater. Sci. Forum* **2012**, 657–660.
33. Walton, S. G.; Muratore, C.; Leonhardt, D.; Fernsler, R. F.; Blackwell, D. D.; Meger, R. A. Electron-Beam-Generated Plasmas for Materials Processing. *Surf. Coat. Technol.* **2004**, *186*, 40–46.
34. Zheng, L.; Ling, L.; Hua, X. F.; Oehrlein, G. S.; Hudson, E. A. Studies of Film Deposition in Fluorocarbon Plasmas Employing a Small Gap Structure. *J. Vac. Sci. Technol., A* **2005**, *23*, 634–642.
35. Ferrari, A. C.; Meyer, J. C.; Scardaci, V.; Casiraghi, C.; Lazzeri, M.; Mauri, F.; Piscanec, S.; Jiang, D.; Novoselov, K. S.; Roth, S.; *et al.* Raman Spectrum of Graphene and Graphene Layers. *Phys. Rev. Lett.* **2006**, *97*, 1874011–1874014.
36. Merel, P.; Tabbal, M.; Chaker, M.; Moisa, S.; Margot, J. Direct Evaluation of the sp(3) Content in Diamond-Like-Carbon Films by XPS. *Appl. Surf. Sci.* **1998**, *136*, 105–110.
37. Walton, S. G.; Lock, E. H.; Ni, A.; Baraket, M.; Fernsler, R. F.; Pappas, D. D.; Strawhecker, K. E.; Bujanda, A. A. Study of Plasma-Polyethylene Interactions Using Electron Beam-Generated Plasmas Produced in Ar/SF6Mixtures. *J. Appl. Polym. Sci.* **2010**, *117*, 3515–3523.
38. OuYang, F. P.; Huang, B.; Li, Z. Y.; Xiao, J.; Wang, H. Y.; Xu, H. Chemical Functionalization of Graphene Nanoribbons by Carboxyl Groups on Stone-Wales Defects. *J. Phys. Chem. C* **2008**, *112*, 12003–12007.
39. Zhou, J.; Liang, Q. F.; Dong, J. M. Enhanced Spin-Orbit Coupling in Hydrogenated and Fluorinated Graphene. *Carbon* **2010**, *48*, 1405–1409.
40. Sofo, J. O.; Suarez, A. M.; Usaj, G.; Cornaglia, P. S.; Hernandez-Nieves, A. D.; Balseiro, C. A. Electrical Control of the Chemical Bonding of Fluorine on Graphene. *Phys. Rev. B* **2011**, *83*, 0814111–0814114.
41. Rafiee, J.; Mi, X.; Gullapalli, H.; Thomas, A. V.; Yavari, F.; Shi, Y.; Ajayan, P. M.; Koratkar, N. A. Wetting Transparency of Graphene. *Nat. Mater.* **2012**, *11*, 217–222.
42. Scocchi, G.; Sergi, D.; D'Angelo, C.; Ortona, A. Wetting and Contact-Line Effects for Spherical and Cylindrical Droplets on Graphene Layers: A Comparative Molecular-Dynamics Investigation. *Phy. Rev. E* **2011**, *84*, 0616021–0616028.
43. Alldredge, E. S.; Badescu, S. C.; Bajwa, N.; Perkins, F. K.; Snow, E. S.; Reinecke, T. L. Adsorption of Nitro-Substituted Aromatics on Single-Walled Carbon Nanotubes. *Phys. Rev. B* **2010**, *82*, 1254181–1254188.
44. Alldredge, E. S.; Badescu, S. C.; Bajwa, N.; Perkins, F. K.; Snow, E. S.; Reinecke, T. L.; Passmore, J. L.; Chang, Y. L. Adsorption of Linear Chain Molecules on Carbon Nanotubes. *Phys. Rev. B* **2008**, *78*, 1614031–1614034.
45. Barone, V.; Casarin, M.; Forrer, D.; Pavone, M.; Sambi, M.; Vittadini, A. Role and Effective Treatment of Dispersive Forces in Materials: Polyethylene and Graphite Crystals as Test Cases. *J. Comput. Chem.* **2009**, *30*, 934–939.
46. Grimme, S. Semiempirical GGA-Type Density Functional Constructed with a Long-Range Dispersion Correction. *J. Comput. Chem.* **2006**, *27*, 1787–1799.
47. Grimme, S. Density Functional Theory with London Dispersion Corrections. *Wiley Interdiscip. Rev. Comput. Mol. Sci.* **2011**, *1*, 211–228.
48. Shirron, J. J.; Zwillinger, D. Standard Math Interactive. *SIAM Rev.* **1999**, *41*, 628–630.
49. Zhu, X.; Wang, H.; Liao, Q.; Ding, Y. D.; Gu, Y. B. Experiments and Analysis on Self-Motion Behaviors of Liquid Droplets on Gradient Surfaces. *Exp. Therm. Fluid Sci.* **2009**, *33*, 947–954.
50. Midey, A. J.; Miller, T. M.; Viggiano, A. A. Kinetics of Ion−Molecule Reactions with Dimethyl Methylphosphonate at 298 K for Chemical Ionization Mass Spectrometry Detection of GX. *J. Phys. Chem. A* **2009**, *113*, 4982–4989.
51. Ewing, R. G.; Eiceman, G. A.; Harden, C. S.; Stone, J. A. The Kinetics of the Decompositions of the Proton Bound Dimers of 1,4-dimethylpyridine and Dimethyl Methylphosphonate from Atmospheric Pressure Ion Mobility Spectra. *Int. J. Mass Spectrom.* **2006**, *255*, 76–85.
52. Kosolapoff, G. M. Dipole Moments of the Lower Dialkyl Alkylphosphonates. *J. Am. Chem. Soc.* **1954**, 3222–3225.
53. Kosolapoff, G. M. Chemistry of Aliphatic Phosphonic Acids 0.2. Dielectric Constants and Viscosity of Some Higher Alkylphosphonates. *J. Am. Chem. Soc.* **1954**, *76*, 615–617.
54. Li, X.; Magnuson, C. W.; Venugopal, A.; Tromp, R. M.; Hannon, J. B.; Vogel, E. M.; Colombo, L.; Ruoff, R. S. Large-Area Graphene Single Crystals Grown by Low-Pressure Chemical Vapor Deposition of Methane on Copper. *J. Am. Chem. Soc.* **2011**, *133*, 2816–2819.
55. Li, X. S.; Cai, W. W.; An, J. H.; Kim, S.; Nah, J.; Yang, D. X.; Piner, R.; Velamakanni, A.; Jung, I.; Tutuc, E.; *et al.* Large-Area Synthesis of High-Quality and Uniform Graphene Films on Copper Foils. *Science* **2009**, *324*, 1312–1314.
56. Kim, K. S.; Zhao, Y.; Jang, H.; Lee, S. Y.; Kim, J. M.; Ahn, J. H.; Kim, P.; Choi, J. Y.; Hong, B. H. Large-Scale Pattern Growth of Graphene Films for Stretchable Transparent Electrodes. *Nature* **2009**, *457*, 706–710.
57. Vanoss, C. J.; Good, R. J.; Chaudhury, M. K. Additive and Nonadditive Surface-Tension Components and the Interpretation of Contact Angles. *Langmuir* **1988**, *4*, 884–891.
58. Stine, R.; Cole, C. L.; Ainslie, K. M.; Mulvaney, S. P.; Whitman, L. J. Formation of Primary Amines on Silicon Nitride Surfaces: A Direct, Plasma-Based Pathway to Functionalization. *Langmuir* **2007**, *23*, 4400–4404.
59. Giannozzi, P.; Baroni, S.; Bonini, N.; Calandra, M.; Car, R.; Cavazzoni, C.; Ceresoli, D.; Chiarotti, G. L.; Cococcioni, M.; Dabo, I.; *et al.* QUANTUM ESPRESSO: A Modular and Open-Source Software Project for Quantum Simulations of Materials. *J. Phys.: Condens. Matter* **2009**, *21*, 395502–395521.
60. We used the psuedopotentials 6.0 C.pbe-van_ak.UPF, F. F. p.-n.-v. U., H 1.0 H.pbe-van_ak.UPF, O 16.0 O.pbe-van_ak.UPF; which were downloaded from http://www.quantum-espresso.org/?page_id=190.
61. Zalalutdinov, M. K.; Robinson, J. T.; Junkermeier, C. E.; Culbertson, J. C.; Reinecke, T. L.; Stine, R.; Sheehan, P. E.; Houston, B. H.; Snow, E. S. Engineering Graphene Mechanical Systems. *Nano Lett.* **2012**, *12*, 4212–4218.
62. Junkermeier, C. E.; Reinecke, T. L.; Badescu, S. C. Highly Fluorinated Graphene. *Condens. Matter*, **2013**, No. arXiv: 1302.6878.